nature physics

Letter

https://doi.org/10.1038/s41567-022-01885-5

# Direct determination of the topological thermal conductance via local power measurement

Received: 27 April 2022

Accepted: 22 November 2022

Published online: 09 January 2023

Check for updates

Ron Aharon Melcer[1,3], Sofia Konyzheva[1,2,3], Moty Heiblum[1] ✉ & Vladimir Umansky[1]

Thermal conductance measurements are sensitive to both charge and chargeless energy flow and are an essential measurement technique in condensed-matter physics. For two-dimensional topological insulators, the determination of thermal Hall (transverse) conductance and thermal longitudinal conductance is crucial for the understanding of topological order in the underlying state. Such measurements have not been accomplished, even in the extensively studied quantum Hall effect regime. Here we report a local power measurement technique that we use to reveal the topological thermal Hall conductance, going beyond the ubiquitous two-terminal conductance. For example, we show that the thermal Hall conductance is approximately zero in the $\nu = 2/3$ particle–hole conjugated state. This is in contrast to the two-terminal thermal conductance that gives a non-universal value that depends on the extent of thermal equilibration between the counter-propagating edge modes. Moreover, we demonstrate the utility of this technique in studying the power carried by the current fluctuations of a partitioned edge mode with an out-of-equilibrium distribution.

The importance of heat flow in electronic systems has been appreciated in recent years as a growing number of thermal transport[1,2] and microscopy[3,4] techniques are being developed. The significance of thermal transport is especially apparent in topologically non-trivial materials. In two-dimensional topological insulators, the bulk of the electron gas is insulating, whereas gapless excitations flow in one-dimensional-like chiral or helical modes next to the sample's edge[5–7]. The nature of the edge modes is a manifestation of the wavefunction in the bulk (due to 'bulk–boundary' correspondence[8]), making edge transport experiments a compelling route for studying bulk properties[9]. In addition to the quantization of the electrical conductance of edge modes, their thermal Hall conductance $\kappa_{xy}T$ ($T$ is the temperature) is also expected to be quantized in units of the thermal conductance quanta $\kappa_0 T = \frac{\pi^2 k_b^2}{3h} T$ ($k_b$ is the Boltzmann constant and $h$ is the Planck constant)[10]. Sensitive to all edge modes, the thermal measurement supplements the electrical one and can distinguish between competing topological phases[11]. The importance of thermal Hall conductance is particularly apparent in topological superconductors, where a half-quantized $\kappa_{xy}$ provides a strong signature of a chiral Majorana mode[12].

The most diverse playground for topological condensed matter is the quantum Hall effect (QHE). The signature of its states is their quantized electrical Hall conductance: $G_{xy} = \nu G_0$, where $G_0 = \frac{e^2}{h}$ is the conductance quantum ($e$ is the electron charge) and $\nu$ is the Landau-level filling, which can be an integer or a simple fraction. Similarly, their thermal Hall conductance coefficient is also quantized: $\kappa_{xy} = \nu_Q \kappa_0$, where $\nu_Q$ is an integer for Abelian QHE states and a fraction for non-Abelian QHE states[11]. For Abelian states, the value of $\nu_Q$ is given by the net number of chiral edge modes, $\nu_Q = n_d - n_u$, where $n_d$ ($n_u$) is the number of downstream (upstream)

[1]Braun Center for Submicron Research, Department of Condensed Matter Physics, Weizmann Institute of Science, Rehovot, Israel. [2]Laboratory of Quantum Materials (QMAT), Institute of Materials (IMX), École Polytechnique Fédérale de Lausanne, Lausanne, Switzerland. [3]These authors contributed equally: Ron Aharon Melcer, Sofia Konyzheva. ✉e-mail: moty.heiblum@weizmann.ac.il

https://doi.org/10.1038/s41567-022-01885-5

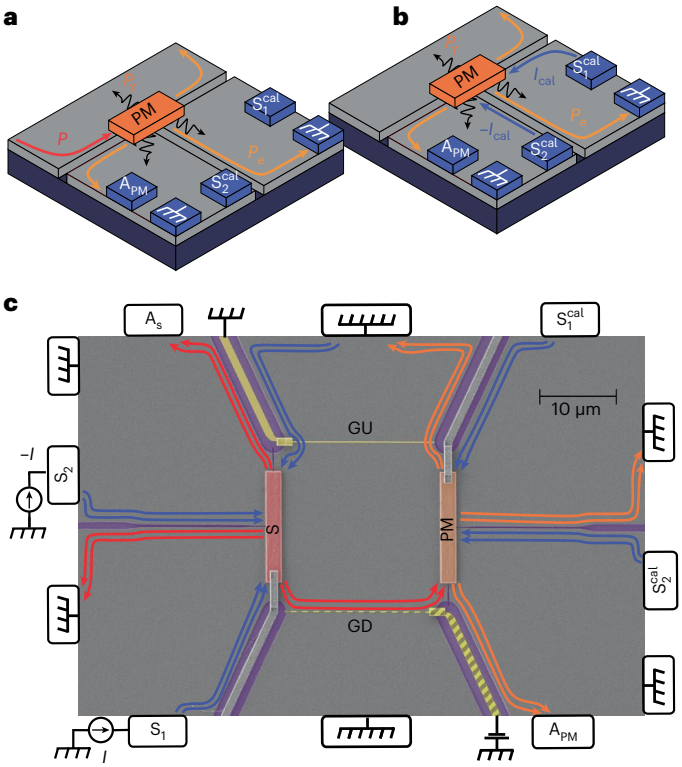


**Fig. 1 | Device configuration for measuring heat transfer. a**,**b**, Measurement configuration of the PM. The PM is a small floating ohmic contact connected to three regions of 2DEG. Measuring the impinging power on the PM (**a**). A heated edge mode ($P$) leaving a heat source (not seen) impinges on the PM, increasing its temperature $T_{PM}$. The resultant J–N noise is measured by the amplifier connected at $A_{PM}$. In equilibrium, the power evacuated from the PM (via phonons $P_\gamma$ and edge modes $P_e$) is equal to the impinging power $P$. Calibration of the PM (**b**). $T_{PM}$ is measured for a known impinging power carried by two d.c. currents $I_{cal}$ and $-I_{cal}$, simultaneously sourced by $S_1^{cal}$ and $S_2^{cal}$, respectively, with $P_{cal}=\frac{I_{cal}^2}{G_{2T}}$. This calibration allows converting $T_{PM}$ into impinging power $P$. **c**, False-colour scanning electron microscopy image of the tested structure. The mesa (grey) is divided into several parts by etched regions (purple). The mesa parts are connected by the floating metallic ohmic contacts, which serve as temperature sources (S; red) and a PM (orange). Both contacts' capacitances to ground are enhanced by an insulated top plate (~0.5 pF; grounded via grey leads). The arrows describe two downstream-propagating edge modes corresponding to the edge structure of $\nu=2$. When currents $+I$ and $-I$ are sourced from $S_1$ and $S_2$, respectively, the source S heats up to temperature $T_S$, measured via J–N noise that is picked up at the source amplifier at $A_S$. In the shown configuration, gate down (GD; dashed yellow) is closed (by applying a negative voltage to the gate), forcing the heated edge modes to flow from S to PM. Gate up (GU; full line coloured yellow) is open, thus grounding the upstream modes (if present). The edge modes heat the PM to a temperature $T_{PM}$, measured by noise at the PM amplifier $A_{PM}$. $T_{PM}$ is later converted into power using a calibration measurement (as shown in **b**).

propagating modes (downstream being the chirality dictated by the magnetic field)[10,13]. The value of $\nu_Q$ (in analogy to $\nu$) is an inherent property of the bulk's topological order[8,13], and is independent of the exact details of the edge structure.

Measuring $\kappa_{xy}$ is essential when studying a QHE state whose topological order is not known. Its value can distinguish between Abelian and non-Abelian topological orders and even discriminate between competing non-Abelian orders[11]. So far, the thermal conductance of QHE states was measured only in a 'two-terminal' configuration, $\kappa_{2T}T$. In such measurements[14–18], a single floating ohmic contact was used as a heat-current source with a known temperature (in analogy to a two-terminal electrical conductance measurement, where one terminal with a known voltage serves as a current source). However, the two-terminal thermal conductance, under some conditions, can be affected by multiple phenomena at the edge and thus differ from topological $\kappa_{xy}$ even if the bulk is thermally insulating ($\kappa_{xx}=0$) (refs. 18,19). The reason for this apparent contradiction is that the quantization of the two-terminal thermal conductance, namely, $\kappa_{2T}=|\kappa_{xy}|$, requires, in addition, the full thermalizing of all counter-propagating (downstream and upstream) edge modes[20]. If the edge modes are not thermally equilibrated, a larger value of $\kappa_{2T}$ is expected. In the vanishing equilibration limit, the upstream and downstream modes carry heat 'in parallel', giving rise to $\kappa_{2T}=\kappa_0(n_d+n_u)$.

States whose edge is known to support topological counter-propagating modes are the particle–hole (P–H) conjugated states[21,22]. These fractional QHE states form when a spin-split Landau level is more than half full, most prominently at fillings of $\nu=\frac{p}{2p-1}$, $p>1$ is an integer, in the lowest Landau level[21,22]. Charge equilibration among counter-propagating edge modes happens fast (in less than 5 μm in GaAs (refs. 19,23)), allowing charge to flow only downstream and renders the upstream modes neutral[24,25]. Quantization of the two-terminal electrical conductance $G_{2T}=G_{xy}$ is measured for the typical length scale of most samples. However, intermode thermal equilibration is less efficient and depends on local microscopic details. As a result, for $\nu=2/3$ (with charge $n_d=1$ and neutral $n_u=1$), the reported values of $\kappa_{2T}$ span from $0.3\kappa_0$ to $2.0\kappa_0$ (whereas $\kappa_{xy}=0$)[15,18,19]. In a recent work, the thermal equilibration length of $\nu=2/3$ was found to even exceed 200 μm in GaAs samples[19].

To reliably measure $\kappa_{xy}$, one must go beyond the two-terminal configuration and separately apply local measurements for the downstream and upstream edge modes. Several local temperature measurement techniques have been reported in the QHE regime; these include quantum dot thermometry[22], partitioned noise thermometry[26,27] and upstream (neutral) noise thermometry[19,28]. However, none of these approaches offers a reliable, independent measurement of the temperature of non-equilibrated counter-propagating modes. We adopt a different approach.

Here we introduce a technique that allows the measurement of the power carried by all types of edge mode—whether integer or fractional—propagating upstream or downstream. Moreover, we can measure the excess power carried by an edge mode, whether in equilibrium with a definite temperature or having a non-equilibrium distribution. This technique opens the path to perform multi-terminal thermal conductance measurements and extract $\kappa_{xy}$ even when the edge modes are unequilibrated.

The key idea of this technique is the conversion of energy carried by the edge modes to the thermal energy of electrons in a floating small metallic reservoir, which serves as a power meter (PM). Once the PM's temperature is calibrated against a known heating power, one can determine the energy absorbed in the PM by measuring its elevated temperature, $T_{PM}$. Importantly, this method relies only on the thermalization of electrons in the floating reservoir and is thus applicable to any two-dimensional topological material as long as ohmic contacts could be implemented along the edge.

In more detail, edge modes deliver power $P$ (which we wish to determine) to the PM and cause its temperature to increase. Consequently, power will leave the heated PM in two ways, $P_{out}=P_e+P_\gamma$ ($P_e$ is the power evacuated via the QHE edge modes and $P_\gamma$ is the power evacuated by lattice phonons). The temperature $T_{PM}$ is determined by the net power dissipated in the PM at equilibrium, that is, $P=P_{out}(T_{PM})$. In our devices, we measure $T_{PM}$ by probing the Johnson–Nyquist (J–N) noise[29,30] in a separate contact $A_{PM}$ (Fig. 1a). Calibration of the PM—meaning, converting the measured temperature into dissipated power—is accomplished with a separate measurement (Fig. 1b). We apply a known power at the PM by sourcing two opposite-sign d.c. currents, $I_{cal}$ and $-I_{cal}$, from two contacts, $S_1^{cal}$ and $S_2^{cal}$, respectively, and

https://doi.org/10.1038/s41567-022-01885-5

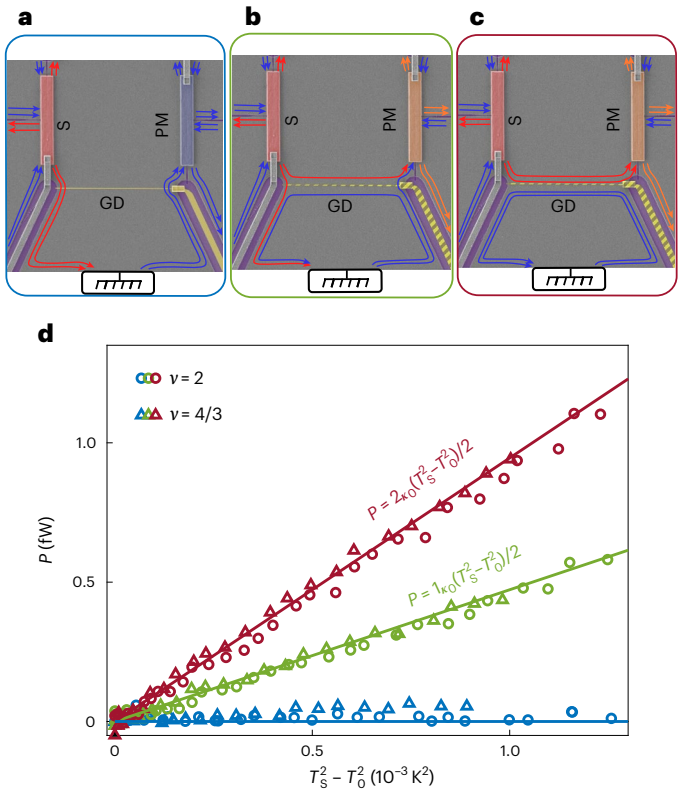


**Fig. 2 | Power carried by downstream modes. a**–**c**, Schematic of the edge mode configurations as a function of the voltage on GD. No gate voltage is applied to GD and the heated modes flow from S to the ground (**a**). Partial pinching of GD allows only one heated mode to be fully transmitted to the PM (**b**). Full pinching of GD. Both heated edge modes emanating from S flow to the PM (**c**). **d**, Power $P$ carried by the downstream edge modes of $\upsilon = 2$ (circles) and $\upsilon = 4/3$ (triangles) as a function of source temperature $T_S$. The different coloured markers correspond to a different number of heated edge modes emanating from S and transmitted across the partly closed GD to arrive at PM. Red, two modes (**c**); green, one mode (inner mode) (**b**); blue, zero modes (**a**). The observed small power in $\upsilon = 4/3$ corresponds to a finite $\kappa_{xx}$. The coloured lines correspond to the theoretical prediction of $P = n_d \frac{\kappa_0}{2}\left(T_S^2 - T_0^2\right)$. The measured data for both integer and fractional states are in good agreement with the prediction. Here $\upsilon = 2$ ($\upsilon = 4/3$) data were measured at a magnetic field of $B = 2.1$ T ($B = 9.6$ T) and base temperature of $T_0 = 11$ mK ($T_0 = 13$ mK).

measure the resulting PM's temperature. No direct current leaves the PM since its potential is zero. An equality $P_{out}(T_{PM}) = \frac{1}{G_{2T}} I_{cal}^2$ defines the equilibrium conditions for the calibration process.

The device (Fig. 1c) consists of two floating small ohmic contacts (each with an area $15 \times 2\ \mu m^2$). Each contact is connected to three regions of the two-dimensional electron gas (2DEG), separated by narrow etched areas. The contact on the left serves as a temperature source (S), and the contact on the right serves as a PM. By sourcing opposite-sign d.c. currents, $I_S$ & $-I_S$, from contacts $S_1$ and $S_2$, respectively, we dissipate electrical power in S, causing its temperature $T_S$ to increase; yet, its potential is zero—ensuring that no current flows to the PM and causes unwanted heating. Two metallic gates, gate down (GD) and gate up (GU), control whether the heated edge modes that emanate from S flow to the PM or to the cold ground.

In the experiment, $T_S$ and $T_{PM}$ are simultaneously probed by measuring the spectral density of the J–N noise by two amplifiers located downstream from S and PM (denoted as $A_S$ and $A_{PM}$, respectively; Fig. 1c). The measured low-frequency noise is proportional to the excess temperature of the heated contact from which the edge modes emanate (it is independent of the edge modes' temperature arriving at the amplifier contact). A separate calibration measurement allows deducting the impinging power on the PM. In a typical experiment, we measure the relation between the arriving power at the PM and the corresponding source temperature.

We start by measuring two 'particle-like' states, the integer QHE state $\upsilon = 2$ and the fractional QHE state $\upsilon = 4/3$. In both, the edge hosts only two downstream edge modes. By changing the gate voltage on GD, we can allow either zero, one or two heated downstream edge modes to flow from S to PM, with the remaining edge modes flowing to the grounded contact (Fig. 2a–c). For the measurement of these states, GU was kept open.

The measured power arriving at the PM is plotted as a function of the source temperature (Fig. 2d) for two, one and zero heated edge modes transmitted to the PM. We find good agreement between the measured power and theoretical expectation for the power carried by each heated mode, that is, $P = \frac{\kappa_0}{2}\left(T_S^2 - T_0^2\right)$, validating our measurement technique. It is worth noting that in particle-like states, heat is carried only by the downstream modes. Thus, the two-terminal heat conductance is equal to the Hall conductance coefficient, namely, the power reaching the PM is $P = \frac{\kappa_{xy}}{2}\left(T_S^2 - T_0^2\right)$. Moreover, unlike in two-terminal measurements, where the temperature must be low enough to avoid substantial heat evacuation by phonons, in our measurement, there is no upper limit on $T_S$ since the phonon contribution is taken into account in the calibration process (of the PM). Moreover, by opening both GD and GU, all the edge modes are grounded, assuring that there is no efficient parallel heat conductance from S to PM (for example, due to a finite longitudinal thermal conductance $\kappa_{xx}$).

The advantage of the multi-terminal approach is particularly apparent in states that support counter-propagating modes, such as P–H conjugated states. It allows independently measuring the power carried by the downstream and upstream modes. Consider a general state with $n_d$ ($n_u$) downstream (upstream) modes. Increasing the temperature of a source contact from $T_0$ to $T_S$ will cause heat to flow downstream and upstream. The excess power carried by the downstream modes after a propagation length $L$ can be written as

$$P_d(L) \equiv \frac{\kappa_d(L)}{2}\left(T_S^2 - T_0^2\right) = \frac{\kappa_0}{2} n_d \left(T_S^2 - T_0^2\right) - P_{d\to u}(L), \qquad (1)$$

where $P_{d\to u}(L)$ is the power backscattered from the hot downstream edge modes to the cold upstream ones along the propagation distance $L$. Similarly, the excess power carried by the upstream modes (at the opposite edge of the sample) is

$$P_u(L) \equiv \frac{\kappa_u(L)}{2}\left(T_S^2 - T_0^2\right) = \frac{\kappa_0}{2} n_u \left(T_S^2 - T_0^2\right) - P_{u\to d}(L), \qquad (2)$$

where $P_{d\to u}$ is the backscattered power from the now hot upstream edge modes to the cold downstream (counter-propagating) modes.

As alluded above, the process of thermal equilibration among the counter-propagating edge modes is technically uncontrolled and is poorly understood. The power reflected to the source can depend on microscopic parameters such as edge potential distribution, edge roughness, modes' velocities, temperature and propagation length. However, under general conditions, the backscattered power is equal in the downstream and upstream sides of the mesa, namely, $P_{d\to u}(L) = P_{u\to d}(L)$ (Supplementary Section 5). One can, thus, extract $\kappa_{xy}$ by separately measuring the power carried by the downstream and upstream modes for a fixed $L$ as

$$P_d - P_u = \frac{\kappa_d - \kappa_u}{2}\left(T_S^2 - T_0^2\right) = (n_d - n_u)\frac{\kappa_0}{2}\left(T_S^2 - T_0^2\right) = \frac{\kappa_{xy}}{2}\left(T_S^2 - T_0^2\right). \qquad (3)$$

We tuned the magnetic field to the $\upsilon = 2/3$ P–H conjugated state. This state supports (in the absence of edge reconstruction) a single

https://doi.org/10.1038/s41567-022-01885-5

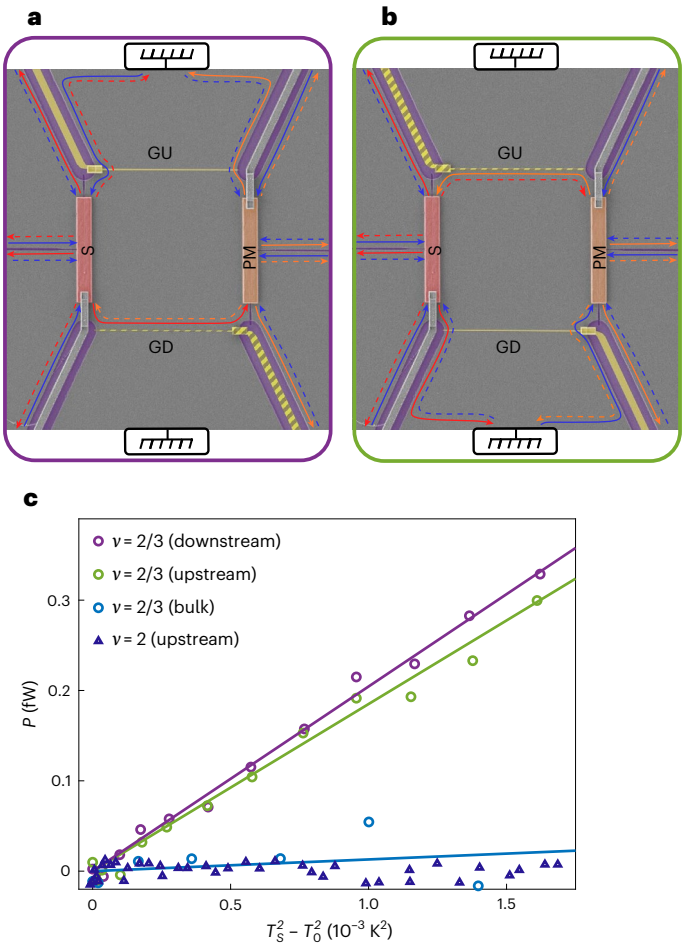


**Fig. 3 | Thermal conductance of the $\nu = 2/3$ P–H conjugated state. a**, Device configurations used to measure the power carried by the downstream mode. **b**, Similar configuration for measuring the power carried by the upstream mode. The arrows mark the edge modes of the $\nu = 2/3$ state: full (dashed) arrow corresponds to the downstream charged mode (upstream neutral mode). In **a**, GD is closed (negative voltage applied on the gate) and GU is open. Excess power is carried to the PM by the heated downstream mode. In **b**, GU is closed and GD is open. Only the upstream mode carries power to the PM. **c**, Downstream power $P_d$ (purple markers) and upstream power $P_u$ (green markers) measured as a function of the source's temperature, in the configuration depicted in **a** and **b**, respectively. By linear fitting $P_{d/u} = \frac{1}{2}\kappa_{d/u}\left(T_S^2 - T_0^2\right)$, we find $\kappa_d/\kappa_0 = 0.43 \pm 0.03$ and $\kappa_u/\kappa_0 = 0.39 \pm 0.03$ (purple and green straight lines, respectively), and consequently, $\kappa_{xy} = \kappa_d - \kappa_u = (0.04 \pm 0.03)\kappa_0$, with the latter in good agreement with the expected $\kappa_{xy} = 0$. The light blue circular markers, linearly fitted with the light blue line, were measured when both GD and GU were open. Here the minute power arriving in the PM (the slope corresponds to $\kappa_{xx}/\kappa_0 = 0.03 \pm 0.02$) is either due to heat propagating through the bulk or due to slight reflection from the 'open' gates. The data were measured at $B = 8.2$ T and base temperature $T_0 = 13$ mK. The dark blue triangles are data points measured at $\nu = 2$ in the upstream configuration (**b**). The vanishing upstream power flow in $\nu = 2$ is expected due to the absence of an upstream neutral edge mode.

downstream charge mode and a single upstream neutral mode corresponding to $\kappa_{xy} = 0$. By closing GD and opening GU, we measure the power carried from S to PM by the downstream side of the mesa, namely, $P_d$ (Fig. 3a). Similarly, we measure the power carried by the upstream side of the mesa by closing GU and opening GD (Fig. 3b). We extract the downstream (upstream) thermal conductance $\kappa_d$ ($\kappa_u$) by the separate linear fitting of the measured downstream (upstream) power arriving at the PM as a function of source temperature squared (Fig. 3c). Here we find $\kappa_d = (0.43 \pm 0.03)\kappa_0$ and $\kappa_u = (0.39 \pm 0.03)\kappa_0$. The thermal conductance of the separately upstream and downstream modes is smaller than that of a single chiral mode ($1\kappa_0$) due to the presence of counter-propagating modes that enable heat to backscatter ($P_{d\to u}(L) > 0$). Applying equation (3) gives $\kappa_{xy} = \kappa_d - \kappa_u = (0.04 \pm 0.03)\kappa_0$, which is very close to the expected value of $\kappa_{xy} = 0$. The two-terminal thermal conductance could also be extracted from the measurement as a sum of the downstream and upstream thermal conductance coefficients, that is, $\kappa_{2T} = \kappa_u + \kappa_d = (0.82 \pm 0.04)\kappa_0$ (Supplementary Section 6). Evidently, only partial thermal equilibration (between the counter-propagating modes) has been reached, indicating that the propagation length is shorter than the thermal equilibration length.

So far, we considered energy carried by edge modes with an equilibrium distribution (the excess power results from an elevated temperature of the modes). Our configuration allows measuring energy transport by edge modes with a non-equilibrium distribution. A simple example of a non-equilibrium distribution is a double-step distribution[31,32]. It can be formed by partitioning a biased edge mode in a quantum point contact (QPC) constriction. The distribution of particles in the outgoing mode will be the statistical sum of the partitioned biased and unbiased incoming modes, namely, $F = tF_V^{FD} + (1-t)F_0^{FD}$, where $F_V^{FD}\left(F_0^{FD}\right)$ is the Fermi–Dirac distribution of the particles in the biased (unbiased) mode and $t$ is the QPC's transmission probability. This out-of-equilibrium distribution supports current fluctuations, with a low-frequency spectral density given by the well-known shot noise formula[33,34] $S_I(f \to 0) = 2e^*It(1-t)\chi\left(\frac{e^*I}{2k_bTG_{2T}}\right)$, where $I$ is the impinging d.c. current, $e^*$ is the particles' charge and $\chi(x) = \coth(x) - \frac{1}{x}$. The excess power carried by the partitioned edge mode has two contributions: the trivial electrical power due to the transmitted direct current, $P_{d.c.} = \frac{1}{2G_{2T}}(tI)^2$, and the power stored in current fluctuations at all frequencies, that is,

$$P_{a.c.} = \frac{1}{2G_{2T}}\int df S_I(f) = \frac{1}{2G_{2T}}I^2t(1-t) \qquad (4)$$

(Supplementary Section 7 provides the derivation of equation (4) and further discussion). Interestingly, the quasi-particle charge $e^*$ and temperature $T$ drop out from the expression. The total power is $P = P_{d.c.} + P_{a.c.} = \frac{1}{2G_{2T}}tI^2$.

The device used to measure the energy carried by the partitioned modes is similar to the one employed above (Fig. 4a–d); however, we no longer use a heated source contact to excite the edge modes. Here we source current $I$ from $S_I$, partition it by a partly pinched QPC (located at the centre of the GD), forming an energy distribution that supports energetic fluctuations. The partitioned beam propagates for approximately 5 μm before being absorbed in the PM.

To measure the energy stored in the current fluctuations, we added a gate arm (GA) that allows pinching off the region to the right of the PM. When the GA is closed, current conservation dictates that the total low-frequency noise that flows to the amplifier is the partitioned shot noise generated at the QPC (Fig. 4a). In this configuration, the heating of the PM will not cause any J–N noise (Supplementary Section 4). However, when the GA is open, J–N noise will be generated on top of the shot noise due to the elevated temperature of the PM (Fig. 4b). By subtracting the shot noise, we are able to isolate the thermal fluctuations and determine $T_{PM}$ (Methods). A calibration process (similar to the one described above) enables the extraction of the impinging power from $T_{PM}$. Here we source unpartitioned current $I_{cal}$ from $S_I$ to the PM (by opening the GD) and measure $T_{PM}$ as a function of dissipating power $P = \frac{1}{4G_{2T}}I_{cal}^2$ (Fig. 4c).

We concentrate on filling $\nu = 2$. At first, the GD was tuned to partition the outer edge mode, whereas the inner one was fully reflected to the ground. From the total power measured by the PM, we subtract the

https://doi.org/10.1038/s41567-022-01885-5

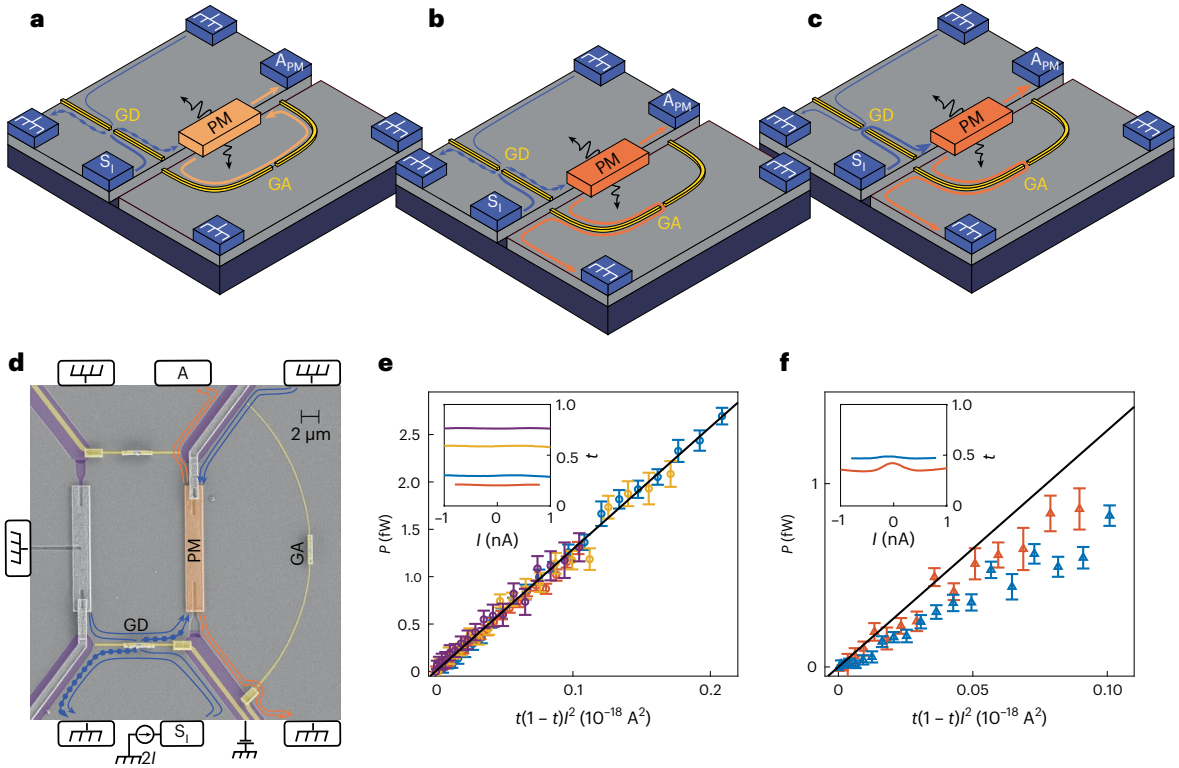


**Fig. 4 | Measuring power carried by out-of-equilibrium edge mode distributions at $\nu = 2$. a–c**, Schematic of the three measured gate configurations. Configuration for shot noise measurement (**a**). A biased edge mode (thick line) is partially transmitted through a 'split-gate' QPC located at the centre of the GD, forming a 'double-step distribution'. The associated shot noise passes through the PM to amplifier $A_{PM}$. Since the gate arm (GA) is closed, no low-frequency fluctuations are added. Configuration to measure the power carried by the double-step distribution (**b**). By opening GA, we enable the J–N noise, which is excited due to PM heating, to be added to the shot noise. The noise is picked up at $A_{PM}$. This noise is used to extract the PM's temperature $T_{PM}$ (Methods). Setup for calibration measurement (**c**). The GD is unbiased (open), and the biased edge modes are fully transmitted towards the PM, heating it by a known dissipated power $P = \frac{I^2}{4G_{2T}}$. Measuring $T_{PM}$ against a known power manifests the calibration process and enables to infer the absorbed power from the measured temperature. **d**, False-colour scanning electron microscopy image of the device used to measure the power carried by out-of-equilibrium distributions. The PM (orange) is connected to two regions of 2DEG, which are otherwise separated by etched regions (purple). The lines represent the edge modes of $\nu = 2$ (thin, unbiased; thick, biased; broken, partitioned beam). **e**,**f**, The a.c. power is carried by the double-step distributions of the outer (**e**) and inner (**f**) edge mode. The power is plotted against the impinging current squared multiplied by $t(1-t)$ (the error bars correspond to statistical uncertainty), and the black line with slope $\frac{h}{2e^2}$ is expected according to equation (4). The different coloured markers correspond to various transmission coefficients of the QPC. The differential transmission is shown as a function of current (insets of **e** and **f**). We find that the power carried by the fluctuations in the outer edge mode agrees well with the expectations without any fitting parameter (**e**). On the other hand, we measured a lower power (**f**) when the inner mode is partitioned.

dissipated d.c. power, thus isolating the power carried by the fluctuations $P_{a.c.}$ (Methods). $P_{a.c.}$ is plotted as a function of impinging current for four different transmission probabilities of the QPC (Fig. 4e). Indeed, the measured power $P_{a.c.}$ agrees well with its expected value without any fitting parameters. This result is independent of any prior knowledge of charge, temperature or even gain of the amplifier (Supplementary Section 4).

However, when the GD was tuned to partition the inner edge mode, a smaller value than the predicted power (by as much as 40%) arrives at the PM (Fig. 4f). The missing energy of the partitioned inner edge mode of $\nu = 2$ is unexpected, as equation (4) is independent of the partitioned charge and temperature. We note that our measurement technique is neither sensitive to charge redistribution along the edge[31] nor to energy transfer to the outer edge mode[35] (since the PM is coupled to both modes). Three possible reasons may account for this discrepancy: (1) the inner mode loses power to the bulk; (2) the PM contact is not coupled well to the inner edge mode; (3) power is lost at the QPC, possibly to excited non-topological neutral modes[36]. We note that the first two reasons are in contradiction with our observation of the correct $\kappa_{xy}$ of $\nu = 2$ (which implies that both edge modes carry the expected power when thermally biased). More research is required to understand this discrepancy, and its relation to other unexplained observations regarding the innermost edge modes, such as vanishing interference and non-Gaussian noise[37].

We have described a method of local power measurement carried by one-dimensional edge modes in the QHE regime. It allows an accurate determination of the topological (not the 'two-terminal') thermal Hall conductance coefficient $\kappa_{xy}$. Our approach utilizes edge transport techniques to measure a fundamental bulk property, independently of the physical properties of the edge itself (for example, the thermal equilibration length or the actual size of the device). This measurement technique is adequate in measuring the power carried by any energy distribution of charge or neutral modes.

## Online content

Any methods, additional references, Nature Portfolio reporting summaries, source data, extended data, supplementary information, acknowledgements, peer review information; details of author contributions and competing interests; and statements of data and code availability are available at https://doi.org/10.1038/s41567-022-01885-5.

## References

1. Pekola, J. P. & Karimi, B. Colloquium: quantum heat transport in condensed matter systems. *Rev. Mod. Phys.* **93**, 041001 (2021).

2. Waissman, J. et al. Electronic thermal transport measurement in low-dimensional materials with graphene non-local noise thermometry. *Nat. Nanotechnol.* **17**, 166–173 (2022).
3. Gomès, S., Assy, A. & Chapuis, P.-O. Scanning thermal microscopy: a review. *Phys. Status Solidi A* **212**, 477–494 (2015).
4. Halbertal, D. et al. Nanoscale thermal imaging of dissipation in quantum systems. *Nature* **539**, 407–410 (2016).
5. Halperin, B. I. Quantized Hall conductance, current-carrying edge states, and the existence of extended states in a two-dimensional disordered potential. *Phys. Rev. B* **25**, 2185–2190 (1982).
6. Wen, X.-G. *Quantum Field Theory of Many-Body Systems: From the Origin of Sound to an Origin of Light and Electrons* (Oxford Univ. Press, 2004).
7. Kane, C. L. & Mele, E. J. Quantum spin Hall effect in graphene. *Phys. Rev. Lett.* **95**, 226801 (2005).
8. Wen, X. G. Gapless boundary excitations in the quantum Hall states and in the chiral spin states. *Phys. Rev. B: Condens. Matter* **43**, 11025–11036 (1991).
9. Wen, X.-G. Topological orders and edge excitations in fractional quantum Hall states. *Adv. Phys.* **44**, 405–473 (1995).
10. Kane, C. L. & Fisher, M. P. A. Quantized thermal transport in the fractional quantum Hall effect. *Phys. Rev. B* **55**, 15832–15837 (1997).
11. Read, N. & Green, D. Paired states of fermions in two dimensions with breaking of parity and time-reversal symmetries and the fractional quantum Hall effect. *Phys. Rev. B* **61**, 10267–10297 (2000).
12. Senthil, T. & Fisher, M. P. A. Quasiparticle localization in superconductors with spin-orbit scattering. *Phys. Rev. B* **61**, 9690–9698 (2000).
13. Cappelli, A., Huerta, M. & Zemba, G. R. Thermal transport in chiral conformal theories and hierarchical quantum Hall states. *Nucl. Phys. B* **636**, 568–582 (2002).
14. Jezouin, S. et al. Quantum limit of heat flow across a single electronic channel. *Science* **342**, 601–604 (2013).
15. Banerjee, M. et al. Observed quantization of anyonic heat flow. *Nature* **545**, 75–79 (2017).
16. Banerjee, M. et al. Observation of half-integer thermal Hall conductance. *Nature* **559**, 205–210 (2018).
17. Srivastav, S. K. et al. Universal quantized thermal conductance in graphene. *Sci. Adv.* **5**, eaaw5798 (2019).
18. Srivastav, S. K. et al. Vanishing thermal equilibration for hole-conjugate fractional quantum Hall states in graphene. *Phys. Rev. Lett.* **126**, 216803 (2021).
19. Melcer, R. A. et al. Absent thermal equilibration on fractional quantum Hall edges over macroscopic scale. *Nat. Commun.* **13**, 376 (2022).
20. Aharon-Steinberg, A., Oreg, Y. & Stern, A. Phenomenological theory of heat transport in the fractional quantum Hall effect. *Phys. Rev. B* **99**, 041302 (2019).
21. Bid, A. et al. Observation of neutral modes in the fractional quantum Hall regime. *Nature* **466**, 585–590 (2010).
22. Venkatachalam, V., Hart, S., Pfeiffer, L., West, K. & Yacoby, A. Local thermometry of neutral modes on the quantum Hall edge. *Nat. Phys.* **8**, 676–681 (2012).
23. Lafont, F., Rosenblatt, A., Heiblum, M. & Umansky, V. Counter-propagating charge transport in the quantum Hall effect regime. *Science* **363**, 54–57 (2019).
24. Kane, C. L., Fisher, M. P. & Polchinski, J. Randomness at the edge: theory of quantum Hall transport at filling $\nu=2/3$. *Phys. Rev. Lett.* **72**, 4129–4132 (1994).
25. Kane, C. L. & Fisher, M. P. A. Impurity scattering and transport of fractional quantum Hall edge states. *Phys. Rev. B* **51**, 13449–13466 (1995).
26. Sivre, E. et al. Electronic heat flow and thermal shot noise in quantum circuits. *Nat. Commun.* **10**, 5638 (2019).
27. Rosenblatt, A. et al. Energy relaxation in edge modes in the quantum Hall effect. *Phys. Rev. Lett.* **125**, 256803 (2020).
28. Kumar, R. et al. Observation of ballistic upstream modes at fractional quantum Hall edges of graphene. *Nat. Commun.* **13**, 213 (2022).
29. Johnson, J. B. Thermal agitation of electricity in conductors. *Phys. Rev.* **32**, 97–109 (1928).
30. Nyquist, H. Thermal agitation of electric charge in conductors. *Phys. Rev.* **32**, 110–113 (1928).
31. Altimiras, C. et al. Non-equilibrium edge-channel spectroscopy in the integer quantum Hall regime. *Nat. Phys.* **6**, 34–39 (2010).
32. Pothier, H., Guéron, S., Birge, N. O., Esteve, D. & Devoret, M. H. Energy distribution function of quasiparticles in mesoscopic wires. *Phys. Rev. Lett.* **79**, 3490–3493 (1997).
33. Martin, T. & Landauer, R. Wave-packet approach to noise in multichannel mesoscopic systems. *Phys. Rev. B* **45**, 1742–1755 (1992).
34. Buttiker, M. Scattering theory of current and intensity noise correlations in conductors and wave guides. *Phys. Rev. B: Condens. Matter* **46**, 12485–12507 (1992).
35. le Sueur, H. et al. Energy relaxation in the integer quantum Hall regime. *Phys. Rev. Lett.* **105**, 056803 (2010).
36. Bhattacharyya, R., Banerjee, M., Heiblum, M., Mahalu, D. & Umansky, V. Melting of interference in the fractional quantum Hall effect: appearance of neutral modes. *Phys. Rev. Lett.* **122**, 246801 (2019).
37. Neder, I., Marquardt, F., Heiblum, M., Mahalu, D. & Umansky, V. Controlled dephasing of electrons by non-Gaussian shot noise. *Nat. Phys.* **3**, 534–537 (2007).

# Methods

## Sample preparation

The ohmic contacts and gates were patterned using standard electron-beam-lithography-based liftoff techniques. The ohmic contact consists of (from the surface and upwards) Ni (7 nm), Au (200 nm), Ge (100 nm), Ni (75 nm) and Au (15 nm), alloyed at 440 °C for 50 s. After the preparation of ohmic contacts, the sample was covered (using atomic layer deposition) by 20 nm $HfO_2$ deposited at 200 °C. The ohmic contact ($HfO_2$) and the gate evaporated on top to form an 'on-chip' capacitor with a capacitance of $c \approx 0.5$ pF. The enhanced capacitance ($\frac{e^2}{c} < k_b T$) guarantees that the contacts are ideal metallic reservoirs[38]. To wire bond the sample, we etched the $HfO_2$ (from the bonding pads) using a buffered oxide etch. The gate electrode consists of 5 nm Ti and 15 nm Au.

## Noise calculation: multi-terminal thermal conductance

In the thermal conductance measurements, the noise measured by the PM amplifier is associated with the temperature of the PM. However, there is noise contribution that originates from the elevated temperature of the source and must be subtracted. We consider the general case where the source is at temperature $T_S$ and the PM is heated to temperature $T_{PM}$. The two-terminal electrical conductance from the source to the PM (or to ground) is $G_{S\to PM}$ ($G_{S\to G}$). The spectral density of the current fluctuations flowing to the PM is given by

$$S_{S\to PM} = 2k_b\alpha\frac{G_{S\to PM}G_{S\to G}}{G_{S\to PM}+G_{S\to G}}(T_S - T_0), \quad (5)$$

where $\alpha$ is a pre-factor that accounts for a smaller noise in P–H conjugated states when edge modes are unequilibrated[19]. For the measured states, we had $\alpha = 1$ for $\upsilon = 2$ and $\upsilon = \frac{4}{3}$ and $\alpha = \frac{3}{4}$ for $\upsilon = \frac{2}{3}$ (Supplementary Section 6). The excess fluctuations are split at the PM contact among all the arms. As a result, the current fluctuations arriving at $A_{PM}$ have two uncorrelated contributions:

$$S_{PM} = \left(\frac{G_{PM\to A}}{G_{PM\to G}+G_{PM\to A}}\right)^2 S_{S\to PM} + 2k_b\alpha\frac{G_{PM\to A}G_{PM\to G}}{G_{PM\to A}+G_{PM\to G}}(T_{PM} - T_0). \quad (6)$$

Here $G_{PM\to A}$ ($G_{PM\to G}$) is the conductance from the PM to $A_{PM}$ (ground). As the temperature of the source is separately measured by means of noise in $A_S$, the first term is known. Equation (6) allows extracting $T_{PM}$ from the noise picked up at $A_{PM}$. Supplementary Section 3 provides a step-by-step analysis of the raw data.

## Noise calculations: double-step distribution

The noise measured at the amplifier has two contributions, the first is the J–N noise emanating from the PM contact due to its elevated temperature and the second term is the shot noise generated at the QPC ($S_{shot}$). Similar to equation (6), we can write the total noise as

$$S_{PM} = \left(\frac{G_{PM\to A}}{G_{PM\to G}+G_{PM\to A}}\right)^2 S_{shot} + 2k_b\frac{G_{PM\to A}G_{PM\to G}}{G_{PM\to A}+G_{PM\to G}}(T_{PM} - T_0). \quad (7)$$

Since we measured at $\upsilon = 2$ and our device has two arms, we can write it in a compact form as

$$S_{PM} = \frac{1}{4}S_{shot} + k_b G_{2T}(T_{PM} - T_0), \quad (8)$$

where $G_{2T} = \frac{2e^2}{h}$. In this experiment, we used only one amplifier; therefore, $S_{shot}$ could not be simultaneously measured. We measured the shot noise separately by closing the GA (Fig. 4a). In this configuration, the noise arriving at the amplifier is the partitioned shot noise generated at the QPC (Supplementary Section 4).

## Power carried by d.c. currents

Considering a 'double-step distribution', the total power dissipated in the PM has two contributions: the power carried by the fluctuations at all frequencies $P_{a.c.}$ and the dissipated part of the power carried by the d.c. currents. The second contribution is subtracted from the measured power to extract $P_{a.c.}$.

When an edge mode carrying current $I$ impinges on a floating contact, it does not dissipate its full power $P^{in}_{d.c.} = \frac{1}{2G_0}I^2$ on the contact. One has to subtract the power carried by the d.c. currents in the outgoing edges as

$$P^{dis}_{d.c.} = P^{in}_{d.c.} - \frac{N}{2}V^2G_0, \quad (9)$$

where $V$ is the contact's potential and $N$ is the number of outgoing edge modes (here $N = 4$). When we partitioned the outer edge of $\upsilon = 2$ with transmission $t$, the dissipated power becomes $P^{dis}_{d.c.} = \frac{3}{8G_0}(tI)^2$. When the inner mode is partitioned, $P^{dis}_{d.c.} = \frac{I^2}{8G_0}(3 + 3t^2 - 2t)$ (Supplementary Section 4.4).

# Data availability

The raw noise measurements (and other) data generated and analysed during the current study are available from the corresponding author on reasonable request. Source data are provided with this paper.

# References

38. Sivre, E. et al. Heat Coulomb blockade of one ballistic channel. *Nat. Phys.* **14**, 145–148 (2018).

# Acknowledgements

We acknowledge C. Spånslätt, J. Park, A. D. Mirlin and K. Snizhko for useful discussions. M.H. acknowledges the continuous support of the Sub-Micron Center staff, the support of the European Research Council under the European Community's Seventh Framework Program (FP7/2007-2013)/ERC under grant agreement number 713351 and the partial support of the Minerva foundation under grant number 713534.

# Author contributions

R.A.M. and S.K. fabricated the devices, performed the measurements and analysed the data. M.H. supervised the experiment and the analysis. V.U. grew the GaAs heterostructures. All authors contributed to the writing of the manuscript.

# Competing interests

The authors declare no competing interests.

# Additional information

**Supplementary information** The online version contains supplementary material available at https://doi.org/10.1038/s41567-022-01885-5.

**Correspondence and requests for materials** should be addressed to Moty Heiblum.

**Peer review information** *Nature Physics* thanks Francois Parmentier and the other, anonymous, reviewer(s) for their contribution to the peer review of this work.